



**UNIVERSITI PUTRA MALAYSIA**

**STRUCTURAL MAGNETIC AND ELECTRICAL PROPERTIES OF  
LA<sub>0.67</sub>CA<sub>0.33</sub>MN<sub>03</sub> PEROVSKITE SYNTHESIZED VIA  
CONVENTIONAL AND CO-PRECIPIATION METHODS**

**HAZAR ALI AHMED ALI SALAMA.**

**FSAS 2004 16**



**STRUCTURAL MAGNETIC AND ELECTRICAL PROPERTIES OF  
 $\text{La}_{0.67}\text{Ca}_{0.33}\text{MnO}_3$  PEROVSKITE SYNTHESIZED VIA CONVENTIONAL AND  
CO-PRECIPIATION METHODS**

**By**

**HAZAR ALI AHMED ALI SALAMA**

**Thesis Submitted to the School of Graduate Studies, Universiti Putra Malaysia,  
in Fulfilment of the Requirements for the Degree of Master of Science**

**June 2004**



## DEDICATION

To:

My Parents.....

My Brothers and sisters

My sister, Umyma .....

Anas  
It's all for you son...

My beloved new born,  
Mohamed

Abstract of thesis presented to the Senate of Universiti Putra Malaysia in fulfilment of the requirements for the degree of Master of Science

**STRUCTURAL MAGNETIC AND ELECTRICAL PROPERTIES OF  
La<sub>0.67</sub>Ca<sub>0.33</sub>MnO<sub>3</sub> PEROVSKITE SYNTHESIZED VIA CONVENTIONAL AND  
CO-PRECIPITATION METHODS**

By

**HAZAR ALI AHMED ALI SALAMA**

**June 2004**

**Chairman: Professor Abdul Halim bin Shaari, Ph.D.**

**Faculty : Science and Environmental Studies**

The structural, magnetic and electrical properties of lanthanum manganites having a nominal composition of La<sub>0.67</sub>Ca<sub>0.33</sub>MnO<sub>3</sub> synthesized via co-precipitation method (COP) following sintering treatments at temperature ranging between 1100°C and 1350°C are reported. XRD pattern showed the monophasic orthorhombic structure of the sample sintered within the above temperature range for a sintering period of 24 hours. The SEM micrographs showed that the grains are well grown and clear grain boundaries are observed. The grain size increased significantly from 1.7µm to 10.3µm as the sintering temperature increases and were well compacted. Large grains growth with layered features is observed in samples sintered at higher temperature. Ferromagnetic-paramagnetic phase transition were observed in the  $\chi'$ -temperature curves for all the sintered samples. The Curie temperature,  $T_c$  shifts to lower temperature as the sintering temperature,  $T_s$  increases. All the samples show the typical ferromagnetic-paramagnetic



phase transition,  $T_c$  in the range 267.9 K~259.7 K. The transport properties show the transition of semiconducting to metallic conductivity at  $T_p$ , the transition occurs within the range 276 K ~ 288 K which is higher compared with the data reported earlier. Based on the semiconducting model,  $\ln(R) \propto (-E_a/K_B T)$  it was observed that the Activation energy,  $E_a$  value ranges from 100.40 to 118.73 meV. The colossal magnetoresistance effect appears at low temperature and the highest value of CMR effect was observed at temperature approaching  $T_p$ . The highest CMR value was observed near the insulator–metal transition. The maximum MR with a value of ~68.2% for  $H = 1.06$  T is obtained in the sample prepared at 1200°C.

The specimens of  $\text{La}_{0.67}\text{Ca}_{0.33}\text{MnO}_3$  prepared via COP method were compared to the specimen prepared by Conventional Powder method (CPM) for samples sintered at 1300°C. XRD spectrum for the samples exhibit orthorhombic distorted and single-phase perovskite structures. The Curie temperature,  $T_c$  and the metal-insulator transition temperature,  $T_p$  were obtained by ac susceptibility and four- point probe techniques. The results showed that  $T_c$  and  $T_p$  were 260 K and 276 K respectively for the COP specimen, which is higher than the results obtained by specimen prepared by CPM with  $T_c$  and  $T_p$  245 K and 246 K respectively. These results are due to the high chemical homogeneity and high density for the COP specimen as compared to the CPM specimen. The CMR for the (COP) specimen is observed near the insulator- metal transition with the value of ~ 56% for  $H = 1.06$  T while for the CPM the CMR value of ~34%

Abstrak tesis yang dikemukakan kepada Senat Universiti Putra Malaysia sebagai memenuhi keperluan untuk ijazah Master Sains

**STRUKTUR, SIFAT MAGNETIK DAN ELEKTRIKAL  $\text{La}_{0.67}\text{Ca}_{0.33}\text{MnO}_3$   
PEROVSKITE YANG DISEDIAKAN MELALUI KAEDAH PEMENDAKAN**

Oleh

**HAZAR ALI AHMED ALI SALAMA**

**Jun 2004**

**Pengerusi: Profesor Abdul Halim bin Shaari, Ph.D.**

**Fakulti : Sains dan Pengajian Alam Sekitar**

Struktur, sifat magnet dan elektrik bagi lanthanum manganites dengan komposisi nominal  $\text{La}_{0.67}\text{Ca}_{0.33}\text{MnO}_3$  yang disediakan melalui kaedah pemendakan diikuti dengan persinteran pada suhu di antara  $1100^\circ\text{C}$  ke  $1350^\circ\text{C}$  dilaporkan. Keputusan XRD menunjukkan struktur fasa tunggal orthorombik pada sampel yang disinter pada suhu tersebut pada kadar 24 jam. Mikrograf SEM menunjukkan saiz butiran yang jelas pembesaranaya dan sempadan butiran yang jelas. Saiz butiran bertambah secara signifikan dari  $1.7\mu\text{m}$  ke  $10.3\mu\text{m}$  berkadar langsung dengan suhu persinteran dan semakin padat. Butiran yang besar dan berlapis kelihatan pada sampel yang disinter pada suhu yang lebih tinggi. Peralihan fasa ferromagnet-paramagnet kelihatan pada lengkungan suhu  $\chi'$  untuk semua sampel yang disinter. Suhu Curie,  $T_c$  beranjak ke suhu yang lebih rendah berkadar songsang dengan suhu persinteran,  $T_s$ . Semua sampel menunjukkan fasa peralihan ferromagnet-paramagnet,  $T_c$  yang tipikal pada julat

267.6 K ~ 259.7 K. Sifat pengangkutan menunjukkan peralihan semikonduktor ke sifat logam pada  $T_p$ , peralihan terhasil pada julat 276 K ~ 288 K di mana ia lebih tinggi daripada data yang sebelumnya. Berdasarkan model semikonduktor,  $\ln(R) \propto (-E_a/K_B T)$  kelihatan nilai tenaga teruja,  $E_a$  pada julat 92.40 ke 118.73 meV. Nilai-nilai ini adalah lebih tinggi dengan signifikan daripada yang didapati. Kesan raksaksa magnetorintangan muncul pada suhu rendah dan nilai yang tertinggi untuk kesan CMR kelihatan pada suhu menghampiri  $T_p$ . Nilai CMR yang paling tinggi kelihatan menghampiri peralihan penebat-logam. Nilai MR maksimum dengan nilai ~68.2% pada  $H = 1.06$  T diperolehi pada sampel yang disediakan pada suhu 1200°C.

Sampel  $\text{La}_{0.67}\text{Ca}_{0.33}\text{MnO}_3$  yang disediakan melalui kaedah pemendakan dibandingkan dengan sampel yang disediakan dengan kaedah tindakbalas pepejal untuk sampel-sampel yang disinter pada suhu 1300°C. Spektrum XRD bagi sampel mempamerkan penyerotan orthorombik dan struktur perovskit fasa tunggal. Suhu Curie,  $T_c$  dan suhu peralihan logam-penebat,  $T_p$  diperolehi dengan kaedah kerintangan a.u dan teknik penduga empat titik. Keputusan menunjukkan  $T_c$  dan  $T_p$  adalah 260 K dan 276 K masing-masing untuk sampel COP, di mana nilainya adalah lebih tinggi daripada keputusan yang diperolehi oleh sampel CPM dengan  $T_c$  dan  $T_p$  adalah 245 K dan 246 K masing-masing. Keputusan ini adalah berkaitan dengan homogeniti dan ketumpatan tinggi pada sampel COP dibandingkan dengan sampel CPM. CMR pada sampel COP diperhatikan menghampiri peralihan penebat-logam dengan nilai ~ 56% untuk  $H = 1.06$  T dan nilai CMR sampel CPM bernilai ~ 34%.

## ACKNOWLEDGEMENTS

Firstly, I am very grateful to “Allah” For giving me the strength, and patient, to complete this research.

My greatest debt to my kind and respectful supervisor, Prof. Dr. Abdul Halim Shaari for his invaluable comments, excellent guidance, feedback, insights and knowledge, continuous supervision, which is greatly appreciated. Without him this thesis would never been completed.

I am highly indebted to all of my supervisory committee, Assoc. Prof. Dr. Zaidan Abdul Wahab and Dr. Noorhana Yahya for their guidance, follow up and knowledge which I received from them. Their help is very much valued and appreciated.

I would like to express my sincerer gratitude to a number of people for their support, collaboration and friendship. I would like to thanks the staff of, Faculty of Science and Environmental Studies UPM, especially the lecturers and staff of Physics Department. A lot of thanks to my entire lab mates whom I worked with them during this research all my colleagues who I worked with them in this lab; especially, Iftetan, Abdullah Chik, Huda, NoorJanah, Masrianis, Walter and Dr. Lim

I'm highly gratefully to all my friends who shared with me the ideas of my project. Special regards Dr. Hamadneh, Khabashi, and Zohra for their efforts and supports.

My fruitfully thanks to Malaysian community in general and UPM family in a particular for their kindness in giving me the opportunity to share the life with them.

My special thanks goes to my father Prof. Ali Salama, my mother for her praying for me and my kids, my lovely sisters and brothers and my sister Umyma who encourage me to complete my study. Thanks to my son Anas for the time he missed his mother.





## TABLE OF CONTENTS

		Page
DEDICATION		iii
ABSTRACT		iv
ABSTRAK		vi
ACKNOWLEDGEMENTS		viii
APPROVAL		ix
DECLARATION		xi
LIST OF TABLES		xiv
LIST OF FIGURES		xv
LIST OF ABBREVIATIONS AND KEY WORD		xix
<b>CHAPTER</b>		
I	<b>INTRODUCTION</b>	1
	1.1 Colossal Magnetoresistance is a shared Phenomenon	7
	1.2 Basic properties	7
	1.3 Applications of the Effect	8
	1.3.1 Magnetic Random access memory (MRAM)	8
	1.3.2 Other Applications	11
	1.4 Research Objective	12
II	<b>BACKGROUND OF COLOSSAL MAGNETORESISTANCE</b>	13
	2.1 Early Theoretical Studies	16
	2.2 Manganites	17
	2.2.1 LaMnO <sub>3</sub>	17
	2.2.2 Doped manganites	18
	2.3 Preparation Methods of Lanthanum Manganite Ceramics	21
	2.3.1 Conventional Method	21
	2.3.2 Sol-Gel Methods	22
	2.3.3 Co-precipitation Methods	24
	2.4 Effect of Heat Treatment on CMR	26
III	<b>THEORY</b>	29
	3.1 Introduction to Magnetism	29
	3.1.1 Diamagnetism	30
	3.1.2. Paramagnetism	30
	3.1.3 Ferromagnetism	31
	3.1.4 Antiferromagnetism	31
	3.2 Magnetic Susceptibility	32
	3.2.1 Curie-Weiss Law	33
	3.2.2 Ferromagnetic susceptibility	33
	3.3 Colossal Magnetoresistance (CMR) Theory	35

3.3.1	Double exchange	35
3.3.2	Jahn-Teller Effect	39
3.3.3	Tolerance Factor	41
<b>VI</b>	<b>METHODOLOGY</b>	<b>44</b>
4.1	Introduction	44
4.2	Materials and Equipment	44
4.2.1	Co-precipitation method (COP)	44
4.2.2	Conventional Powder method (CPM)	47
4.3	Sample Characterization	53
4.3.1	Structural (physical) characterization	53
4.3.2	Microstructure Analysis with Scanning Electron Microscope (SEM)	56
4.3.3	Electrical resistance at various temperatures	57
4.3.4	AC Magnetic Susceptibility Measurement	58
4.3.5	Magnetoresistance Measurements	61
<b>V</b>	<b>RESULTS AND DISCUSSIONS</b>	
5.1	Properties of $\text{La}_{0.67}\text{Ca}_{0.33}\text{MnO}_3$ synthesized via co-precipitation (COP) and Conventional Powder method (CPM) methods	65
5.1.1	XRD Patterns and Lattice Parameters	65
5.1.2	Microstructure Properties	67
5.1.3	Resistance, R and Phase Transition Temperature, $T_p$	69
5.1.4	Magnetic and Electrical Phase Diagram	72
5.1.5	Magnetoresistance	75
5.2	Effect of sintering temperature on LCMO samples prepared by COP method	79
5.2.1	XRD Patterns and Lattice Parameters	79
5.2.2	Microstructure Properties	83
5.2.3	Resistance, R and Phase Transition Temperature, $T_p$	87
5.2.4	Magnetic and Electrical Phase Diagram	91
5.2.5	AC Susceptibility and Curie Temperature, $T_c$	92
5.2.5	Magnetoresistance	96
<b>VI</b>	<b>CONCLUSIONS AND SUGGESTIONS</b>	<b>104</b>
6.1	Conclusion	104
6.2	Suggestions	107
	<b>REFERENCES</b>	<b>109</b>
	<b>APPENDICES</b>	<b>115</b>
	<b>BIODATA OF THE AUTHOR</b>	<b>130</b>

**LIST OF TABLES**

<b>Table</b>	<b>Page</b>
1.1: Comparison of MR Types	5
4.1: Demagnetization factors, $D$ (SI) for cylinders as a function of the ratio of length to diameter, $l/d$	60
5.1.1: Lattice Parameter and Unit- Cell Volume of LCMO specimens	65
5.1.2: The geometric density (mass/volume), theoretical density and porosity of the LCMO samples	67
5.2.1: Lattice Parameter and Unit- Cell Volume of sintered LCMO specimens	80
5.2.2: Activation energies for the LCMO sintered samples	89

## LIST OF FIGURES

Figure	Page
1.1: A summary of the most common types of magnetoresistance (MR)	4
1.2: Temperature dependence of resistivity	6
1.3: MRAM basics	10
2.1: Resistivity of $\text{Nd}_{0.5}\text{Pb}_{0.5}\text{MnO}_3$ as a function of temperature and magnetic fields	15
2.2: Temperature dependence of resistivity of $\text{La}_{2/3}\text{Ba}_{1/3}\text{MnO}_3$ thin film at 0 and 5 T	15
2.3: Schematic structure of an ideal perovskite	18
2.4: Sketched phase diagram of $\text{La}_{1-x}\text{Ca}_x\text{MnO}_3$	20
3.1: Schematic magnetic phenomena in a crystal	32
3.2: Curie- Weiss law shows the presence of paramagnetic phase	34
3.3: (a) Zener (1951) model of double exchange (DE), (b) The mobility of $e_g$ electrons improves if the localized spins are polarized	36
3.4: Schematic diagram of the double exchange mechanism involving two manganese ions and one oxygen ion	38
3.5: Sketch of a spin-canted state	38
3.6: Crystal field lifts the degeneracy of the $d^5$ -electrons of the $\text{Mn}^{3+}$ - ions	40
3.7: Phase diagram at constant doping $x=0.3$ as a function of tolerance factor	43
4.1: Flow chart of $(\text{La}_{0.67}\text{Ca}_{0.33}\text{MnO}_3)$ prepared by co-precipitation method	46
4.2: Sample preparation via Conventional Powder method	48
4.3: Temperature setting for calcinations stage	52
4.4: Temperature setting for final sintering stage	52

4.5:	Schematic illustration of fundamental process in XRD measurement	55
4.6:	Philips X-ray diffraction unit	55
4.7:	JEOL 6400 scanning electron microscope	56
4.8:	Dc resistivity measurements (four-point probe methods)	57
4.9:	Four point probe resistance machine	58
4.10:	Lakeshore AC Susceptometer (model 700)	59
4.12:	Schematic diagram of magnetoresistance measurement	62
4.13:	Schematic diagram of the magnetoresistance setup	63
4.14:	Magnetoresistance measurement system	64
5.1.1:	XRD Spectrum for COP and CPM specimens	66
5.1.2:	SEM image of the fracture surfaces of LCMO samples prepared by COP and CPM	68
5.1.3:	the resistance as a function of temperature for (a) COPspecimens, (b) CPM specimens	70
5.1.4:	Ln (R) as a function of 1/T of LCMO specimens	71
5.1.5:	Temperature dependant of AC Susceptibility of $\text{La}_{0.67}\text{Ca}_{0.33}\text{MnO}_3$ (a) COP specimen, (b) CPM specimen	73
5.1.6:	Inverse susceptibility against temperature of LCMO specimens prepared by CPM and COP	74
5.1.7:	CMR curves as a function of magnetic field of $\text{La}_{0.67}\text{Ca}_{0.33}\text{MnO}_3$ sample Prepared by (a) COP and (b) CPM methods	77
5.1.8:	CMR curve of $\text{La}_{0.67}\text{Ca}_{0.33}\text{MnO}_3$ prepared via COP and CPM samples as a function of temperature at 1.06 Tesla	78
5.2.1:	XRD Spectrum for all the samples of $\text{La}_{2/3}\text{Ca}_{1/3}\text{MnO}_3$ sintered at 1100°C, 1200°C, 1250°C, 1300°C and 1350°C	81
5.2.2:	Lattice parameters and the unit-cell volume of LCMO system	81

5.2.3: geometric density and theoretical density as a function of $T_s$ for LCMO specimens	82
5.2.4: the porosity as a function of $T_s$ for LCMO specimens	82
5.2.5: SEM image of the fracture surfaces of LCMO samples sintered at 1100°C, 1200°C, 1250°C, 1300°C and 1350°C with magnification 2000X and 7,500X	86
5.2.6: Sintering temperature dependence on grain size for $\text{La}_{0.67}\text{Ca}_{0.33}\text{MnO}_3$	86
5.2.7: Temperature dependence of resistance of LCMO samples with $T_s$	88
5.2.8: $T_p$ as a function of $T_s$ of LCMO samples	88
5.2.9: $\ln(R)$ as a function of $1/T$ of LCMO specimens	90
5.2.10: Activation energy, $E_a$ as a function of $T_s$ of LCMO sintered specimens	90
5.2.11: $T_p$ and $T_c$ as a function of $T_s$ of LCMO samples	91
5.2.12: Temperature dependence of a. c Susceptibility of LCMO specimens sintered at 1100°C, 1200°C, 1250°C, 1300°C and 1350°C at $H=10.0$ Oe	93
5.2.13: Sintering temperature, $T_s$ dependence of Curie temperature, $T_c$ for LCMO specimens sintered at 1100°C, 1200°C, 1250°C, 1300°C and 1350°C	93
5.2.14: Inverse susceptibility against temperature of LCMO specimens sintered at 1100°C, 1200°C, 1250°C, 1300°C and 1350°C	94
5.2.15: $T_c$ and $\Theta$ as a function of sintering temperature $T_s$ , for LCMO specimens sintered at 1100°C, 1200°C, 1250°C, 1300°C and 1350°C	95
5.2.16: CMR curve of LCMO sintered specimens as a function of applied magnetic field at 90 K	97
5.2.17: CMR curve of LCMO sintered specimens as a function of applied magnetic field at 100 K	97
5.2.18: CMR curve of LCMO sintered specimens as a function of applied magnetic field at 160 K	99
5.2.19: CMR curve of LCMO sintered specimens as a function of applied magnetic field at 200 K	99

5.2.20: CMR curve of LCMO sintered specimens as a function of applied magnetic field at 260 K	101
5.2.21: CMR curve of LCMO sintered specimens as a function of applied magnetic field at 280 K	101
5.2.22: CMR curve of LCMO sintered specimens as a function of applied magnetic field at 300 K	102
5.2.23: CMR curve of as a function of magnetic field of $\text{La}_{0.67}\text{Ca}_{0.33}\text{MnO}_3$ sample sintered at 1200°C	103
5.2.24: CMR curves of LCMO sintered Samples as a function of Temperature at 1 Tesla.	103

## LIST OF ABBREVIATIONS AND KEY WORDS

$\langle A \rangle$	Average ionic radius
a, b, c	Lattice Parameter
AFI	Antiferromagnetic insulator
AFM	Antiferromagnetic
AMR	Anisotropic Magnetoresistance
CMR	Colossal Magnetoresistance
COP	Co precipitation
CPM	Conventional Powder Method
DE	Double exchange
$d_{hkl}$	Distance between atom and selected $2\theta$
$d_{La-O}$	La-O bond distance
$d_{Mn-O}$	Mn-O bond distance
$E_a$	Activation energy
EMR	Extraordinary Magnetoresistance
f	Frequency.
FMI	Ferromagnetic insulator
GMR	Giant Magnetoresistance
H	Applied magnetic field
hkl	Miller indices
JT	Jahn-Teller
$k_B$	Boltzman constant





LCMO	La-Ca-Mn-O system
M	Magnetization
MI	Metal to insulator
MIT	Metal-insulator transition
MR	Magnetoresistance
PMI	Paramagnetic insulator
$R(0)$	The resistance in zero magnetic field
$R(H)$	The resistance in the magnetic field
S	Spin electron
SEM	Scanning Electron Microscope
T	Temperature in Kelvin
t	Tolerance factor
$T_c$	Curie temperature
TMR	Tunnelling Magnetoresistance
$T_p$	Phase transition temperature.
$T_s$	Sintering temperature.
VLMR	Very Large Magnetoresistance
XRD	X-ray diffraction
$\Theta$	Paramagnetic Curie point
$\chi$	Susceptibility

## CHAPTER I

### INTRODUCTION

Since the discovery of high  $T_c$  superconductivity in copper oxides, in 1986, transition-metal oxides of perovskite structure are receiving much attention. A few years after the initial discovery, in 1993, more excitement greeted reports that certain manganese oxides showed a huge change in electrical resistivity when a magnetic field was applied. This effect is generally known as magnetoresistance, but the resistivity change observed in these oxides was so large that it could not be compared with any other forms of magnetoresistance. The effect observed in these materials "the manganese perovskites" was therefore dubbed "colossal" magnetoresistance to distinguish it from the giant magnetoresistance (GMR) observed in magnetic multilayers and granular films.

The discovery; first reported by researchers at Siemens in Germany and a little later by a group at Bell Labs in New Jersey raised expectations of a new generation of magnetic devices and sensors, and launched a frenetic scientific race to understand the cause of the effect. Today, the promise of great strides in technology remains a challenge, but the perovskites are receiving a lot of attention in their own right (Fontcuberta, 1999).

One reason for this growing interest is the rare-earth manganese oxides, the manganites. In the beginning of the 1990's it was found that some manganites could exhibit a magnetic phase transition close to room temperature, which were accompanied by a

magnetic field driven metal-insulator transition (Chahara et al, 1993, Helholt et al, 1993, Jin et al, 1994).

In general, magnetoresistance is a measure of the change in electrical resistance as function of the magnetic field  $H$  and is usually calculated as:

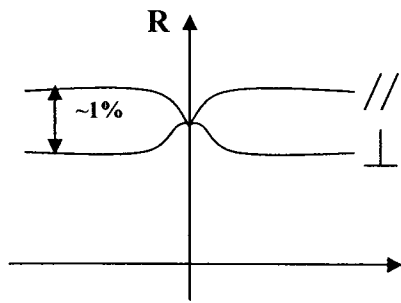
$$MR\% = \frac{R(H) - R(0)}{R(0)} \times 100 \quad 1.1$$

where  $R(H)$  denotes the field dependent resistance and  $R(0)$  the resistance at zero magnetic field.

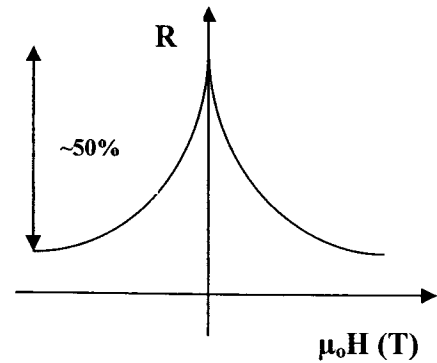
There can be many different physical effects causing magnetoresistance; some of the most common ones are shown in Figure. 1.1. In the mid 19<sup>th</sup> century it was pointed out that the electric resistance in magnetic materials depends on the orientation of an applied magnetic field relative to the orientation of the crystal itself, (Thomson, 1857). A phenomenon given the name *anisotropic magnetoresistance* is shown in Figure. 1.1a. On the other hand, the ordinary magnetoresistance (Figure 1.1b), which is related to the Hall Effect, originates from the impact of the Lorentz-force on moving charge carriers. In absolute numbers, the magnitudes of the anisotropic and the ordinary magnetoresistances are moderate and typically not more than a few percent. In the end of the 1980's it was discovered that multi-layers of magnetic and nonmagnetic metallic materials could show a magnetoresistance of much higher magnitude than previously observed (Baibich et al., 1988). The prefix *giant* was then used to describe the magnetoresistance (Figure 1.1c). Only about half a decade later it was discovered that doped rare-earth manganese oxides by themselves could possess even higher

magnetoresistance (in some cases close to 100%) (Chahara et al., 1993; Helmut et al., 1993; Jin et al., 1994) The physical origin of the magnetoresistance in manganites was completely different from the giant magnetoresistance effect, and hence the term *colossal* was used to describe the effect. The general behavior of colossal magnetoresistance is shown in Figure. 1.1d.

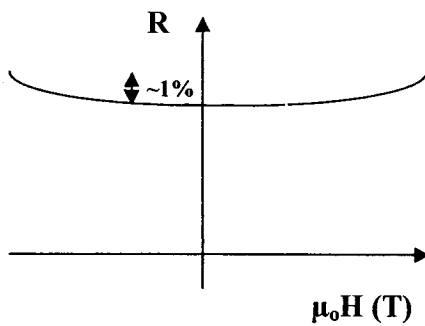
In magnetic tunnel junctions there is another type of magnetoresistance, known as tunnelling magnetoresistance or sometimes junction magnetoresistance, Figure 1.1e and Figure 1.1f. The resistance of a magnetic tunnel junction is lower when the magnetization of the electrodes is parallel than in the antiparallel configuration. It is the ability to switch between these two configurations that is the origin of the tunnel magnetoresistance.



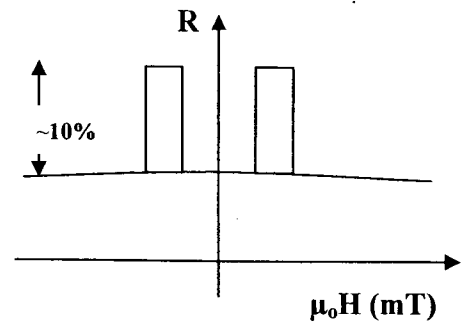
(a) Anisotropic MR



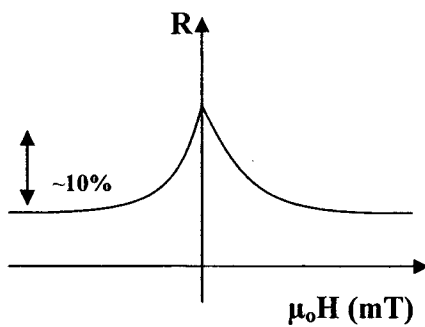
(d) Colossal MR



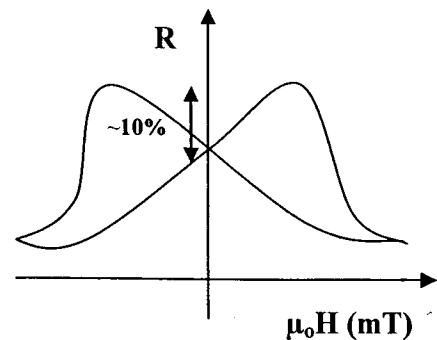
(b) Ordinary MR



(e) Tunnelling MR



(c) Giant MR



(f) Tunnelling MR (bulk)

Figure 1.1: A summary of the most common types of magnetoresistance (MR). The anisotropic, ordinary and colossal MR can be considered as intrinsic effects of the material, while giant and tunnelling MR depend on extrinsic parameters. The tunnelling MR in e) appears in magnetic tunnel junctions, so called spin-valves, while intergrain tunneling in powder and polycrystalline bulk causes a smearing as shown in panel f). Note the different magnitude of the scales.

Anisotropic Magnetoresistance (AMR) measure the change in resistance seen when the current flowing through a sample changes from being parallel to internal magnetization to being perpendicular to it. The materials that exhibit AMR include Permalloy (NiFe) and iron filings. The Tunneling Magnetoresistance (TMR) affect a large change in the electrical resistance upon the application of a magnetic field of two magnetic layers separated by an insulating layer. The Giant Magnetoresistance (GMR) which describes the behavior of materials that have alternating layers of ferromagnetic and nonmagnetic materials deposited on an insulated substrate. The very Large Magnetoresistance (VLMR) effect is seen in homogenous material, and is very similar to GMR.

**Table1.1: Comparison of MR Types**

Type of MR	Increase in Resistance %
MR	1
AMR	20
GMR	200
CMR	100,000